ORIGINAL PAPER

Electrochemical study of intermetallic metal hydride as an anode material for Ni–MH batteries

**Mohamed Tliha · Hamadi Mathlouthi ·
Jilani Lamloumi · Annick Percheron-Guégan**

Abstract The electrochemical behavior of Cobalt-free $LaNi_{3.55}Mn_{0.4}Al_{0.3}Co_{0.4}Fe_{0.35}$ alloy electrode in alkaline solution was investigated using electrochemical impedance spectroscopy (EIS) at different number of charge/discharge cycles. A physicochemical model is developed in order to simulate impedance data. Kinetic parameters are obtained by fitting the electrochemical impedance spectrum performed at different number of cycles. The charge-transfer resistance decreases with increasing number of charge/discharge of cycles, whereas exchange current density and hydrogen diffusion coefficient parameters increase with increasing number of cycles. In addition, the specific surface area of $LaNi_{3.55}Mn_{0.4}Al_{0.3}Co_{0.4}Fe_{0.35}$ alloy electrode increases due to pulverization and the formation of new active sites during charge/discharge cycling. The results of EIS measurements indicate that the performance of the $LaNi_{3.55}Mn_{0.4}Al_{0.3}Co_{0.4}Fe_{0.35}$ metal hydride electrode was markedly improved with increasing number of cycles which is mainly attributed to the increase in the reaction surface area and the improvement in the electrode surface activation.

Keywords Intermetallic hydrides · Electrode materials · Exchange current density · Particle size · Electrochemical reactions

M. Tliha (✉) · H. Mathlouthi · J. Lamloumi
Laboratoire de Mécanique, Matériaux et Procédés,
ESSTT, 5 Avenue Taha Hussein,
1008 Tunis, Tunisia
e-mail: Mohamed.Tliha@esstt.rnu.tn

A. Percheron-Guégan
Laboratoire de Chimie Métallurgique des Terres Rares,
GLVT, 2-8 Rue Henri Dunant,
94320 Thiais Cedex, France

Introduction

The nickel–metal hydride batteries (Ni/MH) based on hydrogen storage alloy electrode have been developed and commercialized because of their inherent advantages over conventional nickel–cadmium batteries, such as high-energy density, high-rate capacity, good overcharge and overdischarge capability, containing no poisonous heavy metals, and no electrolyte consumption during charge/discharge cycling [1–6]. The most recent research in this area has focused on the development of hydride-forming negative electrode materials to increase the electrode capacity and reduce cost. AB_5-type hydrogen storage materials have been extensively studied and applied to commercial production of Ni–MH rechargeable batteries [6–16]. In general, the characteristics of negative electrode of Ni/MH battery, namely metal hydride electrode, is affected not only by the composition, preparation condition, particle size of the alloy powder and the forming conditions of the electrode, but also by the diffusion of hydrogen in the alloy together with charge-transfer reactions on the alloy surface [5]. Among the electrochemical techniques, electrochemical impedance spectroscopy (EIS) technique is a particular useful method to investigate corrosion mechanism and fundamental parameters relating to electrochemical kinetics [17–19].

The aim of this work is to study the electrochemical behavior of the $LaNi_{3.55}Mn_{0.4}Al_{0.3}Co_{0.4}Fe_{0.35}$ metal hydride electrode with different number of cycle by EIS technique. The mechanisms for the electrochemical reactions that occur at the electrode/electrolyte interface are discussed.
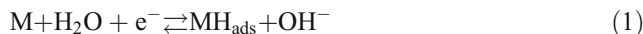
Experimental

A hydrogen storage alloy of the nominal composition $LaNi_{3.55}Mn_{0.4}Al_{0.3}Co_{0.4}Fe_{0.35}$ was prepared through the induction melting of the pure elements followed by an appropriate annealing to ensure a good homogeneity. The purity of starting elemental metals was higher than 99%. The results of the electron probe micro-analysis and the structure characterization by X-ray diffraction (XRD) of this alloy are given in Table 1. The structural characterization shows that this alloy is indexed in the hexagonal $CaCu_5$-type structure (*P6/mmm space group*). The so-called latex technology has been used for the electrode preparation [20]. The alloy is first ground and sieved (to less than 63 μm) in a glove box under argon atmosphere. Ninety percent of this powder has been mixed with 5% of the carbon black (to obtain a good conductivity) and 5% of the polytetrafluorethylene. The mixture (~67 mg) was compressed on the two faces of a nickel grid ($S=0.5$ cm^2), playing the role of a current collector. The electrode in the form of a square contained 60 mg of alloy powder. The thickness of this electrode is 0.5 mm. All the electro-chemical measurements were conducted at room temperature in a conventional three electrode open-air cell, consisting of a working electrode (MH electrode), a Hg/HgO reference electrode, a wire of gold counter electrode, and the electrolyte of the cell was the 7 M KOH solution, using a Voltalab 40 system (Radiometer Analytical) constituted by a Potentiostat-Galvanostat PGZ301. The electrolyte consisted of a 7 M KOH solution which was deaerated by a continuous flow of Argon through the cell. The working potential of the hydride forming the electrode was measured with respect to the Hg/HgO reference electrode.

The EIS measurements were carried out at 10% charging (SOC) for 25 cycles. The EIS data were collected as a function of frequency scanned from the highest of 50 kHz to the lowest of 1 mHz with an ac amplitude perturbation of 5 mV under the open-circuit conditions. The EIS measurements were performed only after the open-circuit potential (i.e., equilibrium potential) was stabilized (i.e., a variation in the potential was less than 1 mV for a period of 1 h). EIS spectra were fitted to equivalent circuit using the software ZSimpWin 3.1.

Results and discussion

The main electrode reactions that occur at a metal hydride electrode are:

$$M+H_2O + e^- \rightleftarrows MH_{ads}+OH^- \quad (1)$$

$$MH_{ads} \rightleftarrows MH_{abs} \quad (2)$$

$$MH_{abs} \rightleftarrows MH_{hyd} \quad (3)$$

where H_{ads}, H_{abs}, and H_{hyd} represent hydrogen adsorbed on the surface, absorbed on the surface and in hydride form, respectively [21]. Reactions 1, 2, and 3 represent the charge transfer at the electrode/electrolyte interface, the transfer of hydrogen atoms from adsorbed to absorbed state at the surface, and the hydrogen atom diffusion in the alloy bulk, respectively. So, the performance of the metal hydride electrode is determined not only by the kinetics of the process occurring at the alloy/electrolyte interface, but also by the rate of hydrogen diffusion within the bulk of the alloy which is believed to play an important role in hydriding and dehydriding processes of the metal hydride electrode.

The EIS is a powerful transient technique to evaluate the interfacial mechanism and the diffusion process of the electrode reaction. Previous studies have shown viable applications of the EIS to analyze the mechanism of hydrogenation/dehydrogenation reactions of the hydride electrodes [22–31]. Most of the authors have been using different equivalent circuits to determine the kinetic parameters, although the impedance diagrams of the metal hydride electrode are relatively similar. In this case, it is difficult to find a suitable equivalent circuit.

Nyquist plots of impedance spectra are reported in Fig. 1a, b for the $LaNi_{3.55}Mn_{0.4}Al_{0.3}Co_{0.4}Fe_{0.35}$ metal hydride electrode at the same state of charge (10% SOC) corresponding to the α-phase solid solution, after a varying number of charge-discharges, during the first 25 cycles. All these spectra consist of a smaller semicircle in the high-frequency region (50 kHz to 20 Hz), a straight line with the angle about 45° in the middle-frequency region (20–1 Hz) and a larger semicircle in the low-frequency region (1 Hz to

Table 1 EPMA analysis, lattice parameters, cell volume of the $LaNi_{3.55}Mn_{0.4}Al_{0.3}Co_{0.4}Fe_{0.35}$ alloy electrode

Compound	EPMA analysis	Cell parameters and volume		
		a (Å)	c (Å)	V (Å^3)
$LaNi_{3.55}Mn_{0.4}Al_{0.3}Co_{0.4}Fe_{0.35}$	$LaNi_{3.55}Mn_{0.40}Al_{0.28}Co_{0.40}Fe_{0.35}$	5.075	4.053	90.41

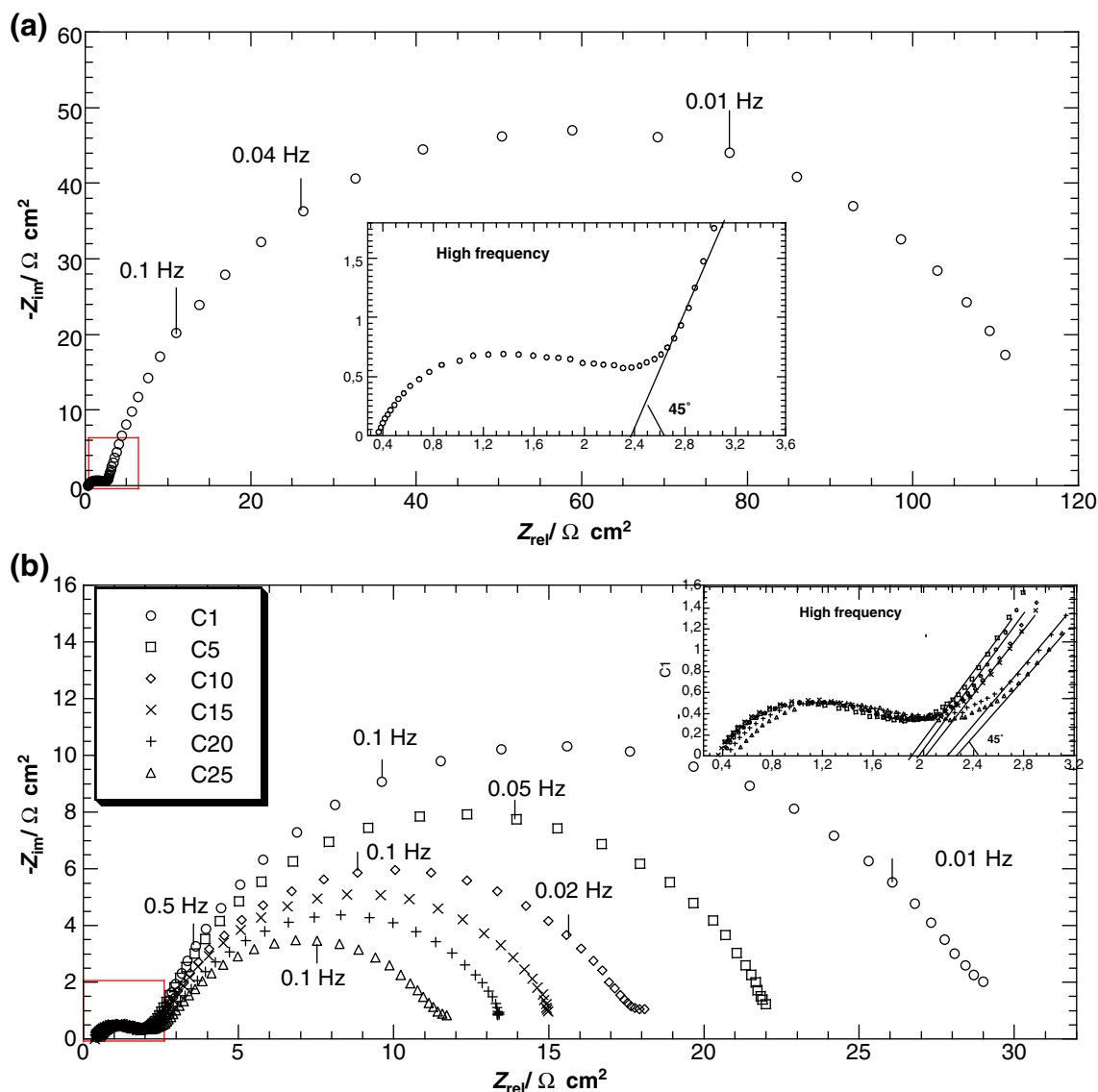*EPMA* electron probe micro-analysis

Fig. 1 Nyquist plots of the LaNi$_{3.55}$Mn$_{0.4}$Al$_{0.3}$Co$_{0.4}$Fe$_{0.35}$ metal hydride electrode at 10% state of charge obtained at different cycles: **a** cycle raw; **b** during the first 25 cycles

1 mHz). However, the interpretations of EIS for MH electrodes have been controversial up to now. The assignment of the small arc in the high-frequency region is not very clear at the moment and is still a matter of controversy. It was first attributed to the contact resistance between the hydrogen storage alloy and the current collector and between the alloys particles [24, 32]. However, recently, based on impedance modeling of the kinetics of metal hydride electrodes, Wang [25] attributed the features at high frequency to the charge-transfer reaction. Experimentally, such a high-frequency small arc was also observed for hydrogen storage alloy ingot [33], which makes its assignment to a contact resistance questionable.

The high-frequency region semicircle can be attributed to the charge-transfer process which takes place at interface [25, 30, 34], the straight line with the angle about 45° in the middle-frequency region is attributed to the Warburg impedance for semi-infinite diffusion [35–37] and the low-frequency region semicircle should be related to the electrode surface process. The experiment results shown in Fig. 1 were fitted by using the software ZSimpWin 3.1. The proposed equivalent circuit used to fit the impedance spectra is given in Fig. 2, where R_e represents the electrolyte resistance, R_{tc} denotes the charge-transfer resistance at the electrode–electrolyte interface, R_{ht} is the hydrogen-transfer resistance, R_{ev} is the resistance of the hydrogen evolution process which characterizes the parasitic process taking place with the
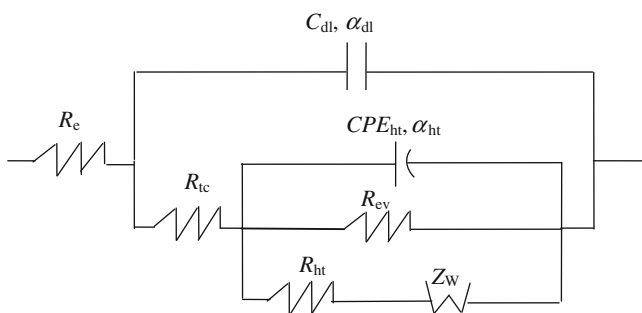
Fig. 2 The proposed equivalent circuit used for simulating the EIS of the LaNi$_{3.55}$Mn$_{0.4}$Al$_{0.3}$Co$_{0.4}$Fe$_{0.35}$ MH electrode

insertion hydrogen in alloys and Z_w is the Warburg impedance for semi-infinite diffusion, C_{dl} is the capacitance of the double layer, CPE$_{ht}$ is modeled as constant-phase element: can be related to the effect of the surface coverage by adsorbed hydrogen on the electrode capacity. CPE is used in this circuit model to take into account the porosity, roughness and inhomogeneity of the surface electrode. Thus, capacitance is deduced from the following relation:

$$CPE = Q(\omega_{max})^{\alpha-1} \tag{4}$$

In this equation, Q is a capacitance parameter, α is a parameter between 0 and 1 and $\omega_{max} = 2\pi f_{max}$, where f_{max} represents the frequency at which imaginary value reaches a maximum on the Nyquist plot.

ZSimpWin 3.1 was used to develop a circuit model from the spectroscopy impedance data. Data was imported from the Voltamaster PGZ301. The modeling process was iterative, using the Chi-square (χ^2) value for the entire model and the percent error values for each circuit component to determine the fit of a given model to the experimental data. Components were chosen using theories from the electrochemical cell studies and using the Boukamp suggestion that each component addition should reduce the χ^2 value by one order of magnitude. Circuit models are presented using the Boukamp representation. The χ^2 value was calculated according to the following algorithm:

Data points and parameters

1. Experimental data point (*frequency*, Z_{real}, Z_{img}) [ω_i, a_i, b_i]
2. Parameters associated with model, $\rho = (\rho_1, \rho_2, \rho_3, ... \rho_m)$
3. Calculated point, [ω_i, $Z'(\omega_i, \rho)$, $Z''(\omega_i, \rho)$]
4. Weighting factors, [ω_i, W_i', W_i'']

Application of statistics

The distance between experimental and calculated points,

$$d_i^2 = \left(a_i - Z'(\omega_i; \rho)\right)^2 + \left(b_i - Z''(\omega_i; \rho)\right)^2$$

The goodness of fit to model,

$$\chi^2 = \sum_{i=1}^{n} \left[W_i' \cdot \left(Z_i'(\omega_i; \rho) - a_i\right)^2 + W_i'' \cdot \left(Z_i''(\omega_i; \rho) - b_i\right)^2 \right],$$

where n is the number of data points.

Weighting options

Unity weighting, $W_i' = W_i'' = 1.0$
Modulus weighting, $W_i' = W_i'' = 1.0/(a_i + b_i)^2$.

The χ^2 value was minimized when the experimental data points correlate with the theoretical data points. This was done by first calculating the difference between the experimental and calculated data points. The difference was squared to give larger variances a greater significance. The difference for all data points were summed and then divided by a weighing factor. According to the literature [38], a χ^2 on the order of 1×10^{-3} or below was acceptable for a given model. The corresponding experimental and theoretical Bode plots are shown in Fig. 3. A good agreement between experimental and calculated data is
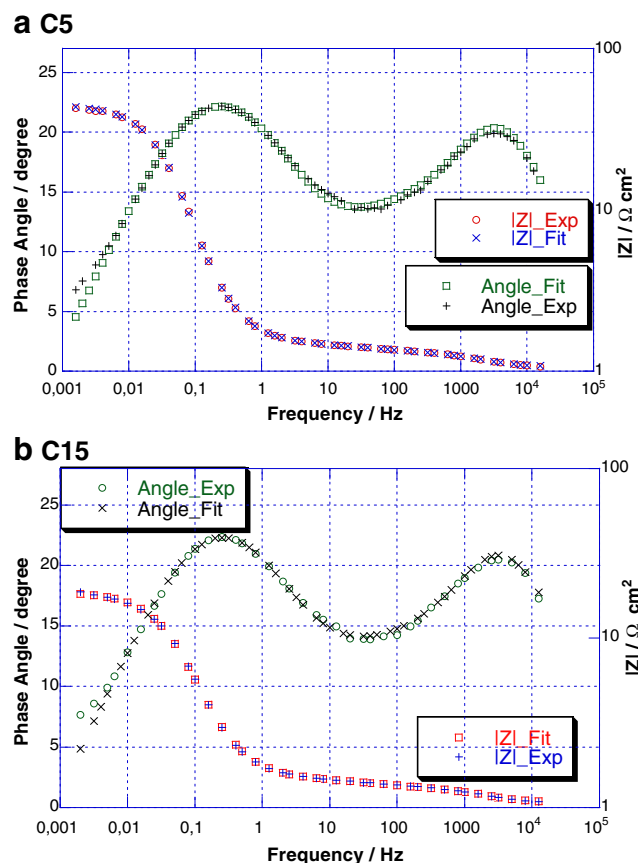

Fig. 3 Results of fitting in Bode diagram of EIS spectra of the LaNi$_{3.55}$Mn$_{0.4}$Al$_{0.3}$Co$_{0.4}$Fe$_{0.35}$ alloy electrode with cycling: **a** at the 5 cycle; **b** at the 15th cycle

observed in the whole frequency range in terms of the present model, where χ^2 was minimized below 10^{-3}. The estimated values of the impedance parameters obtained by the fitting of the experimental data are summarized in Table 2.

The exchange current density (I_0) of the hydrogen storage alloy electrode is commonly used to characterize the catalytic activity for charge-transfer reaction at the electrode/electrolyte interface. The exchange current density, I_0, is calculated from the following equation when an over potential is very small [32]:

$$I_0 = \left(\frac{RT}{nF}\right)\left(\frac{1}{R_{tc}}\right) \qquad (5)$$

Where F is the Faraday constant, n is the number of the exchanged electrons, T is the absolute temperature, R is the gas constant and R_{tc} is the charge-transfer resistance. The calculated values of the charge-transfer resistance, R_{tc}, as a function of the number of cycles are shown in Fig. 4. It can be seen that the charge-transfer resistance, R_{tc}, of the alloy electrode decreases progressively from 2 to 1.36 Ω cm^2 after 15 cycles. The decrease of the charge-transfer resistance of the alloy is mainly attributed to the increase of the new reaction surface areas. The value of the exchange current density is inversely proportional to that of the charge-transfer resistance. The exchange current density vs. the number of cycles for the alloy electrode is shown in Fig. 5. The exchange current density, I_0, of the alloy electrode increases rapidly from 215 to 318 mA g^{-1} after 15 cycles and then reaches 316 mA g^{-1} after 25 cycles. An increase in the exchange current density with the number of cycles reflects the fast hydrogen adsorption process at the interface between MH alloy powder and the electrolyte. Since the exchange current density of the alloy electrode almost remains constant after 15 cycles, this implies that the charge-transfer process at the interface

between the MH alloy powder and the electrolyte is stabilized, i.e., the electrochemical reaction for the hydrogen adsorption at the interface is stabilized. By increasing the number of the charge/discharge cycles, the MH alloy powder will microcrack and be pulverized into micrometer-sized particles because of the expansion of crystal cell through hydrogen absorption and desorption. The microcracks lead to an increase in the reaction surface area and to an improvement in the activation of H adsorption at the electrode/electrolyte interface. The microcracking activation, resulted from an increase in reaction surface area and an improvement in the electrode surface activation, increases the hydrogen exchange current density.

The values of the parameter α_{dl} are close to unity: give the perfect capacitor of the double layer (Table 2). The double-layer capacitance (C_{dl}) increases gradually from 72.2 μF cm^{-2} at the raw material to 96.56 μF cm^{-2} at the 25th cycle (Table 2). The increase of the double-layer capacitance is due to the pulverization of the alloy. The alloy powder was quickly pulverized with increasing the cycle number, and the decrease in particle size leads to a large increase in reaction surface area. These values of C_{dl} are in good agreement with those reported in the literature for intermetallic compounds [37, 39]. The change of the resistance evolution (R_{ev}) is very small with increasing cycle numbers. The results shown in Table 2 reveal that the values of R_{ht} and CPE$_{ht}$ remarkably depend on the cycling. One can see that the hydrogen-transfer resistance, R_{ht}, decreased rapidly with increasing the cycle numbers: 116.5 Ω cm^2 for the raw material, 27.6 Ω cm^2 after one cycle and 10.29 Ω cm^2 after 25 cycles. The larger value of R_{ht} before activation may be ascribed to the low-surface activity. Using Eq. 4, the value of the pseudocapacitance, CPE$_{ht}$, was estimated at each cycle. It can be seen that the value of the CPE$_{ht}$ increases from 85.75 mF cm^{-2} at the raw material to 115.65 mF cm^{-2} at the 25th cycle (Table 2). The

Table 2 The fitted parameters values of the equivalent circuit for the LaNi$_{3.55}$Mn$_{0.4}$Al$_{0.3}$Co$_{0.4}$Fe$_{0.35}$ alloy electrode at different number of cycles

Parameters	Cycle raw	Cycle 1	Cycle 5	Cycle 10	Cycle 15	Cycle 20	Cycle 25
R_e (Ω cm^2)	0.39	0.42	0.42	0.40	0.41	0.50	0.51
R_{tc} (Ω cm^2)	2.01	1.73	1.51	1.38	1.36	1.40	1.37
C_{dl} (μF cm^{-2})	72.2	77.6	81.42	86.0	89.0	92.1	96.56
α_{dl}	1.00	1.00	1.00	1.00	1.00	1.00	1.00
CPE$_{ht}$ (mF cm^{-2})	85.75	104.65	113.70	115.70	113.30	114.20	115.65
α_{ht}	0.87	0.86	0.85	0.85	0.84	0.83	0.82
Y_0 (S s$^{1/2}$ cm^{-2})	0.192	0.230	0.290	0.370	0.390	0.383	0.381
R_{ht} (Ω cm^2)	116.5	27.60	21.08	16.41	14.04	12.33	10.29
R_{ev} (Ω cm^2)	0.69	0.73	0.84	0.90	0.89	0.90	0.92
$D_H \times 10^{-11}$ (cm^2 s^{-1})	0.54	0.77	1.23	2.00	2.22	2.14	2.12
I_0 (mA g^{-1})	215.6	250.5	287	314	318.6	309.5	316.3
$\chi^2 \times 10^{-4}$	4.5	6.4	5.2	3.13	1.73	4.2	1.45

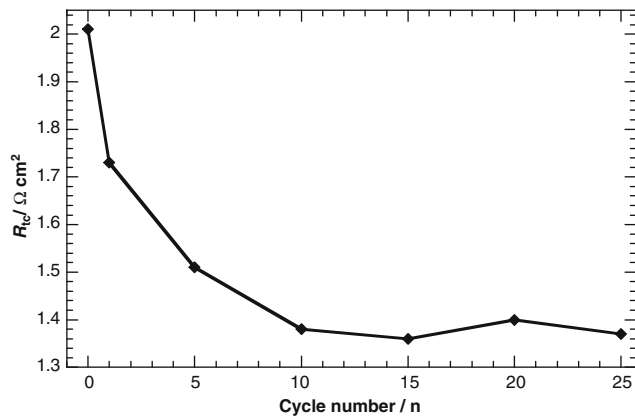**Fig. 4** Charge-transfer resistance of the $LaNi_{3.55}Mn_{0.4}Al_{0.3}Co_{0.4}Fe_{0.35}$ alloy electrode as a function of cycle number

Fig. 6 Hydrogen diffusion coefficient of the alloy electrode with number of cycles

factor α_{ht} shows stable values in the range of 0.82–0.87. These values are different to unity ($\alpha \neq 1$) reflecting a strong change of the surface inhomogeneity with increasing the cycle number.

Hydrogen diffusion coefficient D_H is used to characterize hydrogen diffusion rate in the bulk alloy. The Warburg diffusion impedance is described by the following equations [40, 41]:

$$Z_W = \frac{\delta}{\sqrt{\omega}}(1-j) = \frac{RT}{n^2F^2C_0S\sqrt{2\omega}\sqrt{D_H}}(1-j) \qquad (6)$$

With

$$\delta = \frac{RT}{n^2F^2SC_0\sqrt{2D_H}} \qquad (7)$$

where j is the square root of -1, δ is the Warburg coefficient, n is the number of the exchanged electrons, F is the Faraday constant, S is the geometrical surface of the working electrode (~ 1 cm^2), C_0 is the concentration of diffusing species (~ 0.022 mol/cm^3), R is the gas constant, T is the
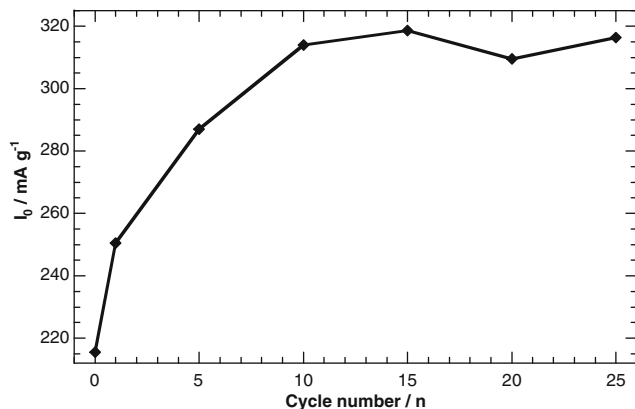
absolute temperature, and D_H is the hydrogen diffusion coefficient. Warburg impedance is also defined by the following equation:

$$Z_W = 1/Y_0(j\omega)^{1/2} = \frac{1}{\sqrt{2\omega}Y_0}(1-j) \qquad (8)$$

Fig. 5 Exchange current density of the $LaNi_{3.55}Mn_{0.4}Al_{0.3}Co_{0.4}Fe_{0.35}$ alloy as a function of cycle number

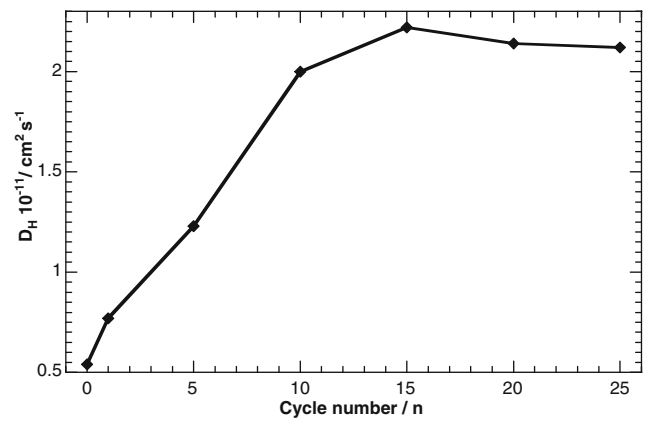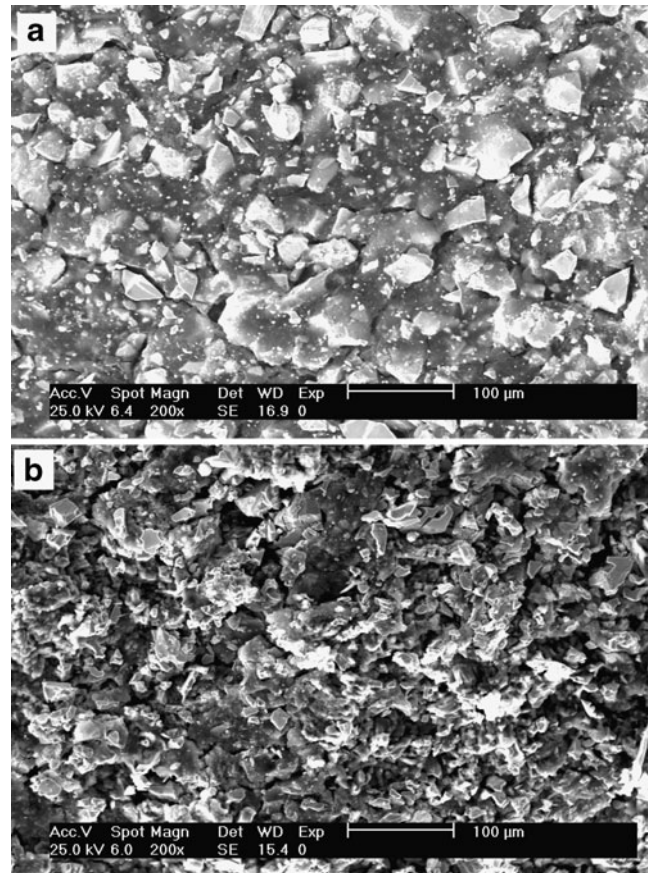**Fig. 7** SEM photograph of the electrode surface: **a** before cycling; **b** after cycling

Where Y_0 is the Warburg admittance, deduced from the fitting of impedance diagrams. Comparing Eq. 8 with Eq. 6, we can obtain:

$$\frac{RT}{n^2F^2C_0S\sqrt{2\omega}\sqrt{D_H}} = \frac{1}{\sqrt{2\omega}Y_0} \quad \Rightarrow \quad \frac{RT}{n^2F^2SC_0\sqrt{D_H}} = \frac{1}{Y_0} \qquad (9)$$

From Eq. 9, the hydrogen diffusion coefficient D_H, can be calculated:

$$D_H = \left[\frac{RTY_0}{n^2F^2SC_0}\right]^2 \qquad (10)$$

The estimated values of the hydrogen diffusion coefficient D_H as a function of the cycle number is shown in Fig. 6. It can be seen that the hydrogen diffusion coefficient increases rapidly from 0.54×10^{-11} to 2.22×10^{-11} cm^{2}s^{-1} after 15 cycles and then almost remains constant. The increase of D_H with increasing number of cycle reflects a decrease in sphere radius of the alloy particle. It is believed that the microcracking of alloy powder in the electrode, due to the hydrogen absorption and desorption processes, results in this decrease in the particle size. After 15 cycles, the radius of the alloy particles is stabilized. These values of D_H are in good accordance with those determined by other techniques [42, 43].

Figure 7a, b present the scanning electron micrographs (SEM) of the LaNi$_{3.55}$Mn$_{0.4}$Al$_{0.3}$Co$_{0.4}$Fe$_{0.35}$ metal hydride electrode before and after activation, respectively. The electrode morphology before the cycling differs from that which underwent the cycles of electrochemical charge and discharge. When charge/discharge cycles are carried out, the average particle size decreases and then remains constant after being fully activated. As seen from SEM results that the average particle size is reduced from 27 μm before cycling to 15 μm after 25 cycles.

The surface roughness factor of the electrode is estimated from the ratio of the measured double-layer capacitance by the EIS and the usual value of the double-layer capacitance. Considering the specific double-layer capacitance C_{dl} the usual value for metal electrodes is about $C_{all}/20$ μF cm^{-2} [44–47], one gets the surface roughness factor, R_f, defined as:

$$R_f = C_{dl}/20\,\mu\text{F cm}^{-2} \qquad (11)$$

The values the surface roughness factor, R_f, of the LaNi$_{3.55}$Mn$_{0.4}$Al$_{0.3}$Co$_{0.4}$Fe$_{0.35}$ alloy electrode increase from 3.61 at the raw material to 4.82 at the 25th cycle. This implies that the surface of the electrode presents a roughness. The real surface area, S_r, can be described as:

$$S_r = S \cdot R_f \qquad (12)$$

Where S is the geometric surface area of the working electrode (~1 cm^2) and R_f is the surface roughness factor.

The values of the real surface area, S_r, increase also from 3.61 cm^2 at the raw material to 4.82 cm^2 at the 25th cycle. This result indicates that the real active area of the electrode is larger than the geometric surface area (not equal to 1 cm^2). With increasing cycle number, the specific surface area increased, and the fresh surface was produced because of the pulverization of the alloy, resulting in improved electrochemical reaction activity and diffusion step by step.

Conclusions

Electrochemical impedance spectroscopy EIS was used to determine the transport and the electrochemical kinetic parameters of the LaNi$_{3.55}$Mn$_{0.4}$Al$_{0.3}$Co$_{0.4}$Fe$_{0.35}$ negative electrode for a Ni/MH batteries at different number of charge/discharge cycles. A physicochemical model is presented to describing the electrochemical behavior of the metal hydride electrode. The results of EIS measurements indicate that the performance of the LaNi$_{3.55}$Mn$_{0.4}$Al$_{0.3}$Co$_{0.4}$Fe$_{0.35}$ metal hydride electrode was markedly improved with increasing number of cycles. With increasing cycle number, the specific surface area increased, and the fresh surface was produced because of the pulverization of the alloy, resulting in improved electrochemical reaction activity and diffusion step by step.

References

1. Willems JJG, Buschow KHJ (1987) J Less-Common Met 129:13
2. Kleperis J, Wocik G, Czerwinski A, Skowronski J, Kopczyk M, Beltowske-Brzezinska M (2001) J Solid State Electrochem 5:229
3. Pan HG, Ma JX, Wang CS, Chen CP, Wang QD (1999) Electrochim Acta 44:3977
4. Anani A, Visintin A, Srinivasan S, Appleby AJ, Lim HS (1992) J Electrochem Soc 139:985
5. Naito K, Matsunami T, Okuno K, Matsuoka M, Iwakura C (1993) J Appl Electrochem 23:1051
6. Ambrosio RC, Ticianelli EA (2004) J Solid State Electrochem 8:532
7. Huang B, Shi P, Liang Z, Chen M, Guan Y (2005) J Alloys Compd 394:303
8. Nathira S, Muralidharan VS, Ahmed Basha C (2009) J Alloys Compd 467:124
9. Seo CY, Choi SJ, Choi J, Park CY, Lee PS, Lee JY (2003) J Alloys Compd 350:324
10. Shi S, Ouyang C, Lei M (2007) J Power Sources 164:911
11. Wang Y, Zhao M, Li S, Wang L (2008) Electrochem Acta 53:7831
12. Feng F, Northwood DO (2005) Int J Hydrogen Energy 30:1367
13. Li F, Young K, Ouchi T, Fetcenko MA (2009) J Alloys Compd 471:371
14. Zhang P, Wie X, Liu Y, Zhu J, Zhang Z, Zhao T (2005) J Alloys Compd 399:270
15. Kim JY, Park CN, Shim JS, Park CJ, Choi J, Noh H (2008) J Power Sources 180:648
16. Li P, Wang XL, Zhang YH, Wu JM, Li R, Qu XH (2003) J Alloys Compd 354:310

17. Mansfeld F, Kendig MW, Tsai S (1982) Corrosion 38:570
18. Silvermann DC, Carrico JE (1988) Corrosion 44:280
19. Juettner K, Lorenz WJ, Kendig MW, Mansfeld F (1988) J Electrochem Soc 135:332
20. Mathlouthi H, Lamloumi J, Latroche M, Percheron-Guegan A (1997) Ann Chim Sci Mat 22:241
21. Zheng G, Popov BN, White RE (1996) J Electrochem Soc 143:834
22. Lim C, Pyun SI (1993) Electrochim Acta 38:3645
23. Kuriyama N, Sakai T, Miyamura H, Uehara I, Ishikawa H, Iwasaki T (1992) J Electrochem Soc 139:172
24. Zhang W, Kumar MPS, Srinivasan S, Ploehn HJ (1995) J Electrochem Soc 142:2935
25. Wang C (1998) J Electrochem Soc 145(6):1801
26. Zheng G, Haran BS, Popov BN, White RE (1999) J Appl Electrochem 29:361
27. Li X, Dong H, Zhang A, Wie Y (2006) J Alloys Compd 426:96
28. Deng C, Shi P, Zhang S (2006) Mater Chem Phys 98:514
29. Wang Y, Lu ZW, Wang YL, Yan TY, Qu JQ, Gao XP, Shen PW (2006) J Alloys Compd 421:236
30. Gao X, Liu J, Ye S, Song D, Zhang Y (1997) J Alloys Compd 253:515
31. Gao XP, Zhang W, Yang HB, Song DY, Zhang YS, Zhou ZX, Shen PW (1996) J Alloys Compd 235:225
32. Kuriyama N, Sakai T, Miyamura H, Uehara I, Ishikawa H (1993) J Alloys Compd 202:183
33. Yuan A, Xu N (2001) J Alloys Compd 322:269
34. Yang H, Zhang Y, Zhou Z, Wei J, Wang G, Song D, Cao X, Wang C (1995) J Alloys Compd 231:625
35. Xu YH, He GR, Wang XL (2003) Int J Hydrogen Energy 28:961
36. Mathlouthi H, Khaldi C, Ben Moussa M, Lamloumi J, Percheron-Guegan A (2004) J Alloys Compd 375:297
37. Ben Moussa M, Abdellaoui M, Khaldi C, Mathlouthi H, Lamloumi J, Percheron-Guegan A (2005) J Alloys Compd 399:269
38. Cui XY, Martin DC (2003) Sens Actuators B Chem 89:92
39. Mathlouthi H, Lamloumi J, Percheron-Guegan A, Baddour R, Pereira JR (2003) Phys Chem News 11:54
40. Yuan X, Xu N (2001) J Alloys Compd 329:115
41. Xu P, Han XJ, Zhang B, Lv ZS, Liu XR (2007) J Alloys Compd 436:369
42. Zheng G, Popov BN, White RE (1995) J Electrochem Soc 142:2695
43. Geng M, Han J, Feng F, Northwood DO (1999) J Electrochem Soc 146:3591
44. Kerner Z, Pajkossy T, Kibler LA, Kolb DM (2002) Electrochem Commun 4:787
45. Pajkossy T, Kolb DM (2001) Electrochim Acta 46:3063
46. El-Aziz AM, Hoyer R, Kibler LA, Kolb DM (2006) Electrochim Acta 51:2518
47. Bard AJ, Faulkner LR (1983) Electrochimie: principes, methodes et applications. Maison, Paris